Overcurrent Protection with Semiconductor Device Protection for Li-Ion Battery Management System in Electric Bicycles

Nisai H. Fuengwarodsakul[1],
Waraporn Puviwatnangkurn[2], and **Bundit Tanboonjit**[3], Non-members

ABSTRACT

This paper presents a design concept of an overcurrent protection for Li-Ion battery pack used in electric bicycles. This overcurrent protection scheme is implemented as a part of a battery management system (BMS). In addition to the conventional protection of Li-Ion battery packs, the proposed concept extends the protection to cover also semiconductor devices in the motor converter from short-circuit faults and overloading. The protection scheme was developed based on i^2t current-time protection characteristics in order to obtain interrupting characteristics in a similar way to the conventional overcurrent protection devices like circuit breaker or fuse. The developed protection concept was implemented by adapting the software algorithm of a high-grade battery management system platform without any hardware adaptation. The existing discharging MOSFETs are employed as an electronic circuit breaker mechanism for cutting-off the circuit. The functionality of the proposed concept was successfully validated by experimental results.

Keywords: battery management systems, electric vehicle, batteries.

1. INTRODUCTION

Nowadays the interest in using electric vehicle is significantly growing due to environmental concerns and political supports. Besides electric cars and shuttle buses, light electric vehicles, such as electric bicycles, electric scooters, etc., become more popular and have experienced an extreme growth. A good example of electric bicycle culture is China. It is estimated that there are now more than 120 million of electric bicycles in China, whereas the number in the late 1990s is only about tens of thousands [1].

In the beginning, lead-acid battery has been widely used as an energy storage source in electric bicycles owing to the cost advantage. In the last ten years, Li-Ion battery has been introduced to high-grade electric bicycles or scooters, of which requirements, i.e. weight, size or power density, cannot be fulfilled by lead-acid batteries [2]. Fig. 1 shows an example of a high-grade electric-power-assist bicycle using Li-Ion battery.

Although Li-Ion batteries can magnificently outperform lead-acid batteries but they are highly sensitive to the operation outside their recommended Safe Operating Area (SOA) in terms of voltage, current and temperature, which could lead to shortened life-time, damage and explosion risk. To achieve high performance, safety and long life-time, an electronic circuit called Battery Management System (BMS) is necessarily applied in order to monitor the Li-Ion battery pack and to protect it from any abnormal conditions, such as overcharging, overcurrent and too high temperature [3]. Fig. 2 shows a diagram of an entire electric propulsion system of an electric bicycle. The BMS is a crucial interfacing unit between the battery pack and other components, i.e. motor converter.

In general, the BMSs for Li-Ion battery pack mainly focus on the protection of the battery in terms of life-time, cell-balancing, undervoltage, safety operation, etc. [3-7]. The conventional overcurrent protection in the instant BMS IC is normally implemented by current-level comparators with delay times. In electric bicycles with Li-Ion battery, the overcurrent protections in the BMS are usually designed without special concerns for other devices in the system, especially, the switching MOSFETs which are the most sensitive devices inside the motor converter. The BMS designer normally configures the overcurrent protection characteristic in the conventional BMSs just for protecting the battery.

In case of short-circuit fault in the converter or on the motor side as depicted in Fig. 2 (number 3 and 4), MOSFETs are frequently damaged by overcurrent, since the protection by fuse or conventional BMS reacts too slow to cut-off in time. These types of overcurrent fault frequently happen, when the insulator of the motor windings is damaged by overheat or humidity during operation or by mishandling during service. As a result, the bicycle owner has to spend more for the replacement of both converter and mo-

Manuscript received on July 21, 2014 ; revised on August 25, 2014.

[1] The authors are with Department of Electrical and Software Systems Engineering The Sirindhorn International Thai-German Graduate School of Engineering, King's Mongkut University of Technology North Bangkok, Thailand, Email: nisai.f.epe@tggs-bangkok.org

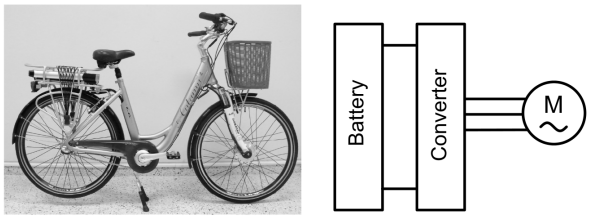

Fig.1: *Example of High-grade electric Bicycle (electric-power-assist bicycle).*

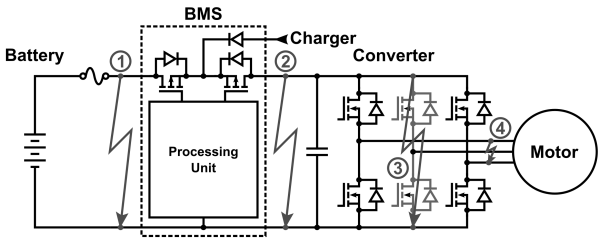

Fig.2: *Electric Propulsion System of considered electric Bicycle and possible Short-circuit Fault Locations.*

tor, although the fault origin comes from the motor side only.

Even though fuses with semiconductor protection capability are commercially available, but they are too expensive for a cost-sensitive application like electric bicycles [8-11]. Another method using thyristor was also proposed but it is suitable only for large DC supply systems [12]. For solving the aforementioned problem, this paper presents the design concept and implementation of an overcurrent protection with semiconductor protection based on the existing components in a high-grade BMS system. The discharging MOSFETs will be employed as an interrupting mechanism in a similar way to an electronic DC circuit breaker [13-14]. The concept of electronic circuit breaker provides a fast interruption and offers flexibility for configuring the protection characteristics. For the simplicity in protection coordination, the protection characteristic of the proposed concept will be based on the conventional i^2t characteristic of thermal fuses. The protection algorithm will be mainly implemented by digital signal processing so that the configuration of the protection characteristic can be easily reconfigured by software. The proposed concept will be compared with a conventional protection concept which is implemented by comparators with delay times and available in commercial BMS ICs.

The following sections describe the development of the proposed protection concept. At the end, the functionality of the developed scheme was verified by experimental results. The technical specifications of the considered electric bicycle system are summarized

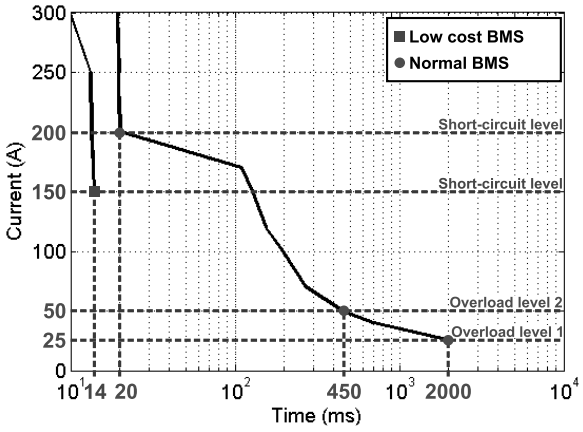

Fig.3: *Interrupting Time of conventional BMS (commercially available).*

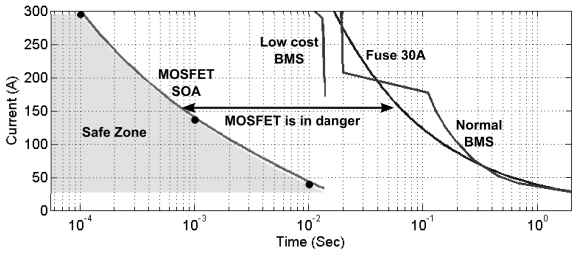

Fig.4: *Safe Operating Current-time Range of MOSFET IRF2807 (extracted from datasheet, at Junction temperature of 175° C) in Comparison to Protection Characteristics of Fuse and Conventional BMSs.*

in the following as the design information.

- Motor: BLDC, 36V, 250W
- Converter: Input voltage 36V, 720VA
- Fuse: Automotive fuse (ATOF) 30A
- Battery: Li-Ion(LiFePO4), 36V, 10Ah Max. discharging current 20A (continuous) Max. discharging current pulse 30A $<$ 30 s

2. CONCEPT OF OVERCURRENT PROTECTION

2.1 BMSs and current protection by i^2t characteristic

In general, BMSs for small electric vehicles like electric bicycles can be classified into three levels according to functions and the hardware implementation as follows,

1 Low-grade BMS using analog circuits for cell balancing and overcurrent protection with simple comparators

2 Medium-grade BMS using instant BMS IC for cell balancing and overcurrent protection with time-delayed comparators. This type is popular in terms of cost and performance.

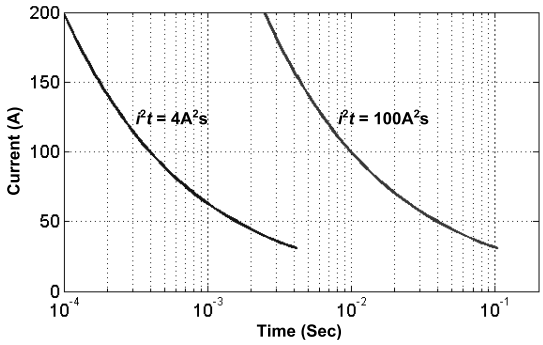

Fig.5: *Adjustment of Interrupting Time by Changing* $i^2t_{threshold}$.

3 High-grade BMS using the same hardware as medium-grade BMS but an additional processing unit is applied for further complicated functions, e.g. battery capacity estimation, communication with other systems. This type of BMS is not popular due to its high cost. It is usually found in high-grade products. Nevertheless, the overcurrent protection is still done by the instant BMS IC.

As a conclusion, the overcurrent protection used in the conventional BMSs, which are commercially available, can be divided into 2 types,

1 Overcurrent protection with simple comparator using analog circuit denoted here as "low cost BMS"

2 Overcurrent protection with time-delayed comparator using instant BMS IC denoted here as "Normal BMS". Even in a high-grade BMS, the overcurrent protection is done by the instant IC as well.

The characteristics of both overcurrent protections are depicted in Fig. 3. The proposed concept in this paper is introduced to replace the overcurrent protection of the instant BMS IC by using a digital signal processing unit. Therefore, this concept can be implemented in a high grade BMS, in which a processing unit is already available. For the medium-grade BMS, the hardware adaptation is required.

The major goal of the proposed overcurrent protection scheme is to protect the semiconductor devices in the motor converter from any damages caused by short-circuit faults. Fig. 2 shows four possible fault locations in the system. The fault number 1 at the internal battery terminals inside the battery pack rarely happens. Nevertheless, a fuse is applied and provides the protection in this area. The fault number 2 occurs between the output of the BMS and the input of the motor converter. This fault type does not damage the MOSFETs and the BMS can normally cut-off in time without any harm to components in the system. The fault number 3 and 4 are the cases in which MOSFETs conduct high short-circuit current and could be destroyed. When these fault types occur, the BMS must manage to cut-off very fast before any components are destroyed.

From the literature survey, most of BMSs have been already equipped with a short-circuit fault protection. However, they are not designed with the consideration of protecting the semiconductor devices in the motor converter. Fig. 3 shows the measured interrupting time of the conventional BMSs. Using those BMSs, the typical cut-off time for short circuit fault is in the range of 14-20 ms, whereas the short-circuit threshold is set between 150-200A. This is the typical range which is equivalent to the discharging rate of 15-20C of a 10Ah Li-Ion battery. Note that the $LiFePO_4$ battery could deliver the short-circuit current up to 25C (250A)[15]. However, the amplitude of the short-circuit current also depends on the battery condition and the impedance of the short circuit path.

As the starting point of the design, the recommended safe operating area of the MOSFETs in the used motor converter (IRF2807) is considered. Fig. 4 shows the boundary of the safe operating current-time area of MOSFETs IRF2807 at the junction temperature of 175°C (extracted from datasheet)[16-18]. On the right hand side, the current-time characteristic of the used 30A fuse is also depicted. It can be seen that, for the range of short-circuit current over 140 A, the MOSFET will be only safe when the cut-off time is shorter than 1 ms. Therefore, it is clear that neither the conventional BMS nor the 30A fuse can protect the MOSFETs from damages. In order to protect the MOSFETs, the BMS must cut-off with a current-time response which is faster than the MOSFET safe operating area boundary.

The current-time characteristics of fuse described by a function of i^2t have been widely accepted for conventional overcurrent protections in electrical circuits [19]. i^2t also represents the energy generated by the fault current. Therefore, the cut-off current-time characteristic of the developed overcurrent protection is designed based on the i^2t characteristics. By setting a value of $i^2t_{threshold}$, the resulting current-time characteristic is derived by (1).

$$\int_{t-T}^{t} i^2_{measured} = i^2t_{threshold} \tag{1}$$

where T = considered time period.

From (1), the i^2t product is the integral sum of the measured current i^2 in a window period of T prior to the present time instant t. When the i^2t product exceeds the given threshold $i^2t_{threshold}$, the circuit will be cut-off. Fig. 5 shows the adjustment of the current-time curve by changing $i^2t_{threshold}$. By increasing $i^2t_{threshold}$, the current-time protection curve is shifted to the right hand side for the slower response. For the faster response, the $i^2t_{threshold}$ should be reduced. Note that the end point on the right side of the curve is determined by the size of the

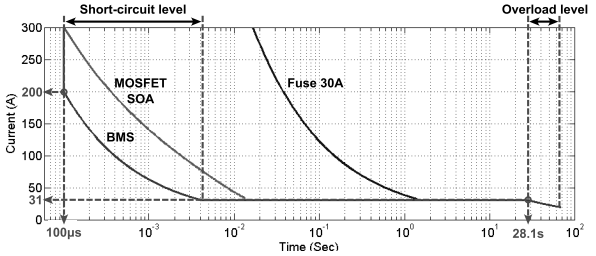

Fig.6: *Coordination between Short-circuit Protection and Overload Protection.*

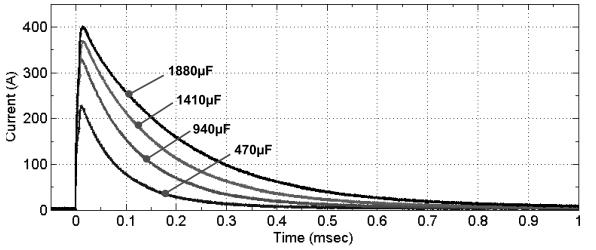

Fig.7: *Discharging Current under Short-Circuit by Different DC-link Capacitors with Initial Voltage of 50V.*

window period T. The calculation of i^2t will be implemented by digital signal processing. Therefore, the current-time protection curve can be adjusted with ease by only changing parameters in software.

2.2 Coordination between Short-Circuit Protection and Overload protection

The short-circuit protection usually has to respond very fast at high current levels in the order of ms, whereas the overload protection works much slower in the order of tens seconds. An inappropriate coordination between these two protections could lead to malfunction or nuisance trip. Therefore, attention should be paid for designing the coordination between these two protections.

Table 1: *Summary of Parameters for Current-Time Protection Characteristics.*

Parameter	Short-circuit	Overload
$i^2t_{threshold}$	$4A^2s$	$27{,}000A^2s$
Current range	$\geq$31A-200A	20A-31A
Interrupting time	4.2ms-100μs	67.5s-28.1s

For the short-circuit protection, the $i^2t_{threshold}$ is set at $4A^2s$, so that its current-time protection characteristic is under the SOA of MOSFETs shown in Fig. 6. The maximum detected current is 200A limited by the current sensor. The shortest detection time is 100μs which is the sampling time period of the A/D converter. Since the battery can be overloaded up to 30A (recommended by manufacturer), the protection curve of the short-circuit protection will end at 31A. The further lower current range from 20-30A will be covered by the overload protection.

The datasheet of the battery defines that the battery can supply the maximum continuous discharge current of 20A (2C). For overloading in short time, it should not supply 30A (3C) longer than 30 s so the $i^2t_{threshold}$ of the overload level is set at $27{,}000A^2s$. The time-current characteristic curve of $27{,}000A^2s$ is shown on the right hand side of Fig. 6. The shortest overloading time is 28.1 s at the average current of 31 A, whereas the longest overloading time is 67.5 s. Table 1 summarizes the parameters for current-time protection characteristic for the considered BMS.

2.3 Short-Circuit Current supplied by DC-Link Capacitor

For short-circuit faults during operation, not only the battery pack supplies the short-circuit current but also the DC-link capacitor, as shown in Fig. 2. Therefore, the influence of DC-link capacitor on the fault current should be investigated. An experiment was carried out to measure the short-circuit current supplied by the DC-link capacitor at different capacitance values at the voltage of 50 V. Fig. 7 shows the results of this experiment. Note that electric bicycles use the nominal DC voltage in the range of 24-48V.

It can be seen that the stored energy can be discharged with high pulse current in a short time period (shorter than hundreds μs). Therefore, the total fault current is the superposition of the battery current and this capacitor current. Since the capacitor current decays very fast, the i^2t integral of the capacitor current does not play a significant role and can be neglected, if the peak current is not too high. This peak current relates to the capacitance of the DC-link capacitor. As an empirical value extracted from experiments, this peak current should be kept under 250 A which corresponds to the capacitance range of 500-700μF, so that there is no risk of damage caused by the peak current supplied by the DC-link capacitor. Therefore, the converter designer should be careful in selecting the DC-link capacitor. The considered converter has the DC-link capacitor of 470μF, which makes the peak current from the capacitor lower than 250A. Therefore, the effect of the DC-link capacitor can be neglected in this design consideration.

2.4 Advantages of the proposed protection concept

The first major advantage is the idea to configure the overcurrent protection to cover the MOSFETs in the motor converter as well. This minimizes the damage of the motor converters, when a fault occurs on motor lines. The second major advantage of the proposed i^2t overcurrent protection concept against the

conventional overcurrent protection in BMSs (comparators with delay times) is the flexibility for the BMS designer to adjust the protection characteristic by changing only parameters in software. In contrast, the protection characteristic of the conventional protection in BMS ICs has a complicated adjustment by changing the RC circuit.

The third advantage is the flexibility of the protection coordination. Using the i^2t scheme, the system designer can configure the protection coordination among the components in the system easily (in case the system has more components such as lightings), so that the protection in the subcomponents will take action before the protection of the BMS. With an appropriate overcurrent protection coordination, the fault location in the system can be identified with ease.

3. IMPLEMENTATION

The proposed concept of the overcurrent protection was implemented on a high-grade BMS for Li-Ion battery packs used in electric bicycles. The hardware structure is shown in Fig. 8. The fundamental functions are the followings,

1. Cell balancing function: The cell balancing function is implemented by the instant BMS IC. It prevents the battery cells from unbalanced voltage during charging. When any battery cell reaches the full charge threshold voltage, that cell will be partly discharged by a bleeding resistor.
2. Overvoltage and undervoltage protection: This function is implemented by the processing unit. The pack voltage and the cell voltages are detected. The processing unit will send the cut-off command to the charge or discharge switches to cut-off the circuit when overvoltage or undervoltage occurs. The operation with undervoltage does not cause a sudden damage but it leads to shortened life-time of battery, whereas the operation with overvoltage leads to sudden damage of battery cells.
3. Overcurrent protection: The current sensor is implemented by a shunt resistor. This type of current sensing is better than the hall current sensing when measuring high short-circuit current beyond the normal range. The linearity and accuracy of the hall current sensor can be affected by magnetic saturation caused by high short-circuit current over the measurement range.

In this paper, the overcurrent protection is the major focus. To implement the proposed overcurrent protection, the existing discharging switch in the BMS is employed as the cut-off mechanism. It consists of three P-channel MOSFETs connected in parallel with low conduction losses. In order to avoid damages to these discharging MOSFETs, the total current rating of this MOSFET group must be much greater than the expected short-circuit current.

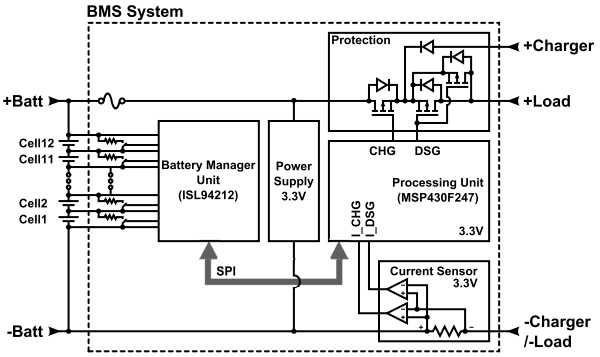

Fig.8: *Hardware Structure of Developed BMS.*

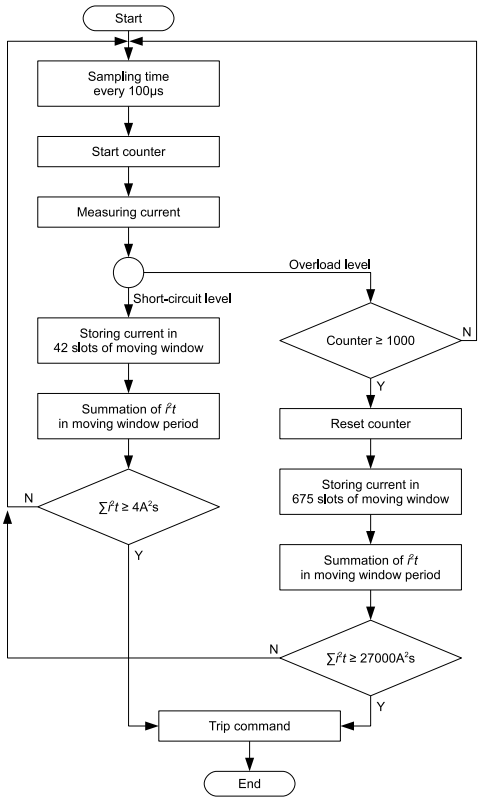

Fig.9: *Flowchart of Proposed Protection Algorithm.*

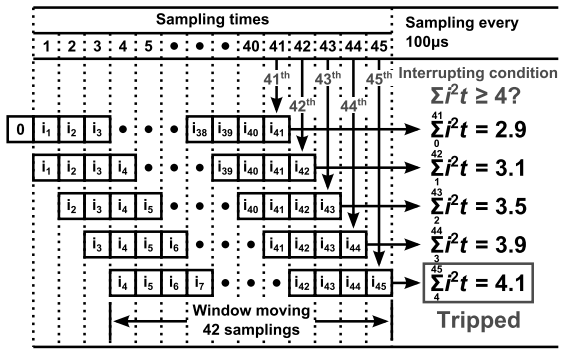

Fig.10: *Example of i^2t Calculation for Short-circuit Protection using Moving Window Method.*

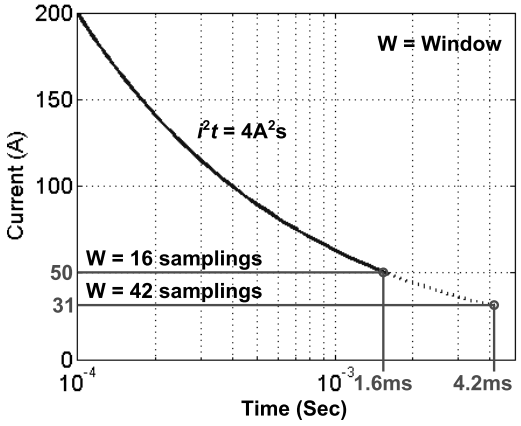

Fig.11: *Effect of Number of Sampling to Current-ime Protection Curve.*

Moreover, attention should be paid also in the layout of the MOSFET circuit, so that the current during transients is equally shared among these discharging MOSFETs. The conducting paths to these three MOSFETs should have the same impedance.

A BMS instant IC ISL94212 is responsible for the cell balancing and cell voltage measurement, whereas the microcontroller MSP430F247 is the main signal processing unit of the system. This microcontroller is a low-power consumption type, which is important for the BMS application, since the power consumption of the BMS circuit is considered as the self-discharge power of the battery pack as well. The battery current is measured by a shunt resistor. The sampling time of the A/D converter is 100 μs. The calculation is carried out by 16-bit integer.

The proposed protection algorithm is described by the flowchart in Fig. 9. For both short-circuit protection and overload protection, the i2t sum is calculated using a moving window of time period in a similar way. The only difference is the size of the window and the value of $i^2t_{threshold}$.

Fig. 10 illustrates how the i^2t sum is calculated by the moving window method. It shows the structure of the memory array occupied by 42 data slots. As the time is passing by, the oldest value will be deleted and replaced by the newest value. As soon as the i^2t sum exceeds the threshold value, the processing unit will send a cut-off command to the discharging MOSFETs.

The size of the window determines the number of data slots and the required memory resource of the processing unit. Fig. 11 illustrates how the number of sampling influences the current-time protection curve. The right end point of the curve will be shortened, when the number of data sampling is reduced. In this case, the longest time period for the short-circuit protection is 4.2 ms. Therefore, the number of data slots is set to 42. For the overload protection, the required memory resource will be extremely large, when sampling at 100μs (675,000 data). The sampling time is enlarged to 100 ms by applying a counter in order to reduce the memory requirement to only 675 slots

4. EXPERIMENTAL VALIDATION

For validating the functionality of the proposed overcurrent protection concept, an experiment setup was built as shown in Fig. 12. A short-circuit fault was simulated using a DC contact relay with high-current rating. From Fig. 12, the relay is connected to make a short-circuit path between the motor lines (line-line fault). To cause a short-circuit fault, the relay will be energized by a DC power supply and the contact of the relay will be closed. In this fault case, two MOSFETs of the converter (the left-top and the right bottom ones) conduct the short-circuit current as shown in Fig. 12.

4.1 Functionality of proposed Concept

A commercial BMS was also tested to be compared with the proposed concept under the same condition. For this test the MOSFETs were warmed up to approximately 60∘C for emulating the operating temperature. During the test, the drain-source voltages of the MOSFETs are recorded in order to observe their conditions.

Fig. 13 shows the cut-off performance of a commercial BMS. After the fault occurred, the battery current has an overshoot nearly 200A. During the fault period the battery current gradually decreased due to the increased resistance of the MOSFETs, which can be observed from the increased voltage drop across the MOSFETs, V_{DS}. At the time point of 11.5 ms after the fault starting time, the lower MOSFET was broken down leading to a sudden voltage drop. Afterwards, the damage of the upper MOSFET followed. The BMS has cleared the fault after 15 ms, which is obviously too late to save the MOSFETs.

Fig. 14 shows the cut-off performance of the proposed scheme, which takes only a total clearing time of 1.04 ms. Actually, the BMS detected the fault current and sent the trip signal after the fault occurred at 380 μs. The cut-off circuit takes further delay of 660 ms for clearing the fault. The major factor for this cut-off delay is the turn-off delay time of the MOSFETs. To ensure a short turning-off time of the MOSFETs, the charge in the Gate-Source capacitance must be quickly drained. The fast turn-off can be obtained by circuit technique. However, this turn-off delay is evitable.

By repeating the test 10 times, the result shows that the MOSFETs in the motor converter are 100% protected. None of them was destroyed by the short-circuit current. (Noticed from their V_{DS}, only the upper MOSFET is measured). One interesting point

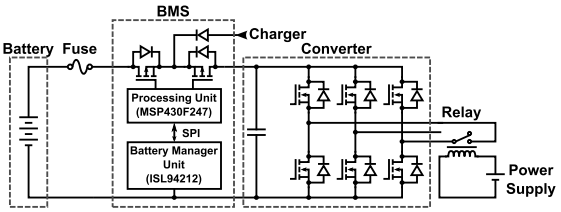

Fig.12: *Experiment Setup for Testing Short-circuit Fault.*

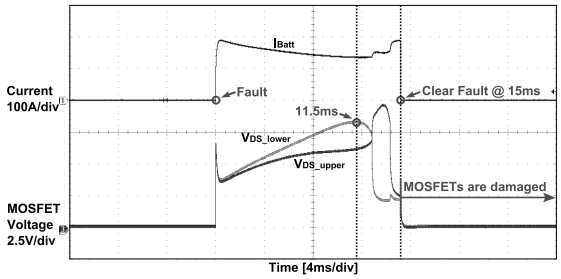

Fig.13: *Interrupting Time of Commercial BMS.*

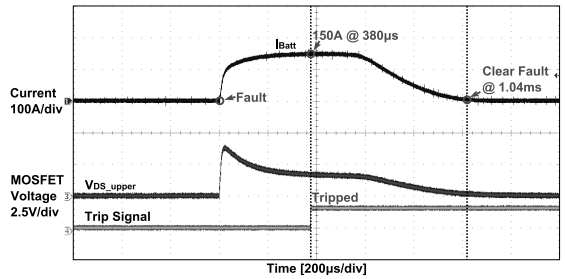

Fig.14: *Interrupting Time of Proposed BMS.*

is that the peak of the fault current is only 150A which is lower than that of the commercial BMS. The reason is that the cut-off action starts very soon before the current reaches the overshoot to nearly 200A. Note that the short-circuit path consists of reactance and resistance, the current slope and peak are limited by the impedance of the short-circuit path.

This implies that the proposed concept can also help minimize the overshoot of the fault current by the fast cut-off. As a conclusion the proposed concept offers a very fast cut-off response which is sufficient to fully protect the MOSFETs when short-circuit occurs.

4.2 Verification of Accuracy

The accuracy of the interruption response should be investigated, since it will be affected by the quantization error due to digital sampling by A/D and by the integer calculation when using a microprocessor with limited computational resources.

The interruption response was tested at different overcurrent levels based on the current-time protec-

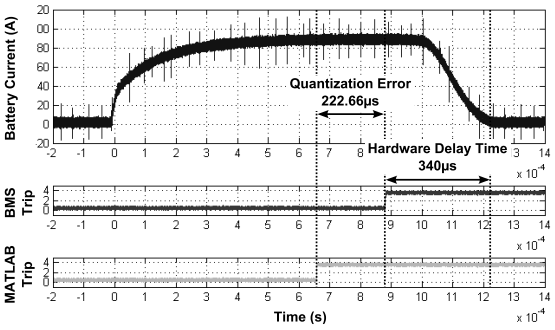

Fig.15: *Short-circuit Protection at 84A.*

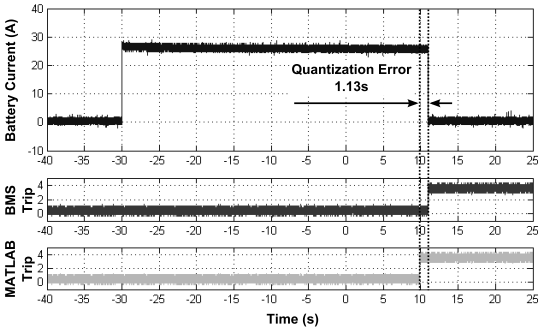

Fig.16: *Overload Protection at 25A.*

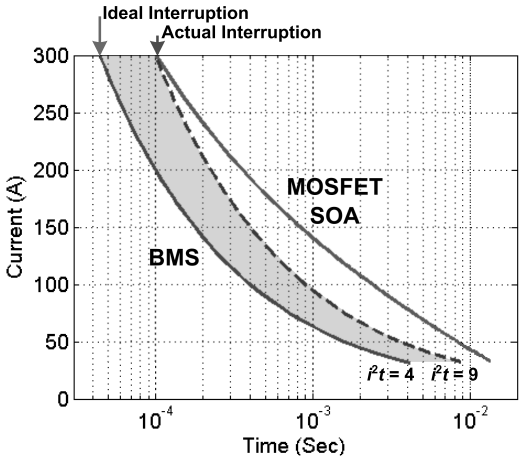

Fig.17: *Actual Protection Curve in Comparison to MOSFET SOA Curve.*

tion curve as shown in Fig. 6. The overcurrent protection algorithm is divided into two levels, the overload level (20-31A) and the short-circuit level ($\geq$31-200A).

For this test, the battery was loaded at different current levels. The interrupting time of the implemented protection algorithm in each current level will be compared with the interrupting time calculated by the software MATLAB. The current curve is measured and input into MATLAB in order to determine the actual interrupting time at which the i^2t sum by

Table 2: *Summary of Parameters for Current-Time Protection Characteristics.*

Overcurrent level(A)		BMS trip (s)	MATLAB trip (s)	Delay by Quantization error (s)	Recalculated $i^2t_{threshold}$ (A^2s)
Overload	25	41.00	39.87	1.13	27,752.40
Short circuit	40	2.72m	2.2m	516μ	7.14
	60	1.80m	1.46m	344μ	6.34
	84	884μ	661μ	222μ	7.29
	110	636μ	453μ	182μ	8.21
	122	444μ	350μ	93μ	7.95

an accurate calculation in MATLAB becomes greater than $i^2t_{threshold}$.

Fig. 15 shows the accuracy test of the short-circuit protection. The delay of the trip signal caused by the quantization error is about 222μs, whereas the hardware delay is about 340μs. The quantization error is also presented in the overload protection as shown in Fig. 16. Table 2 summarizes the quantization error at different overcurrent levels. Table 2 shows that the actual trip signal tends to be slightly delayed by the quantization error and corresponds to a higher equivalent value of $i^2t_{threshold}$.

The recalculated $i^2t_{threshold}$ in Table 2 are in the range of 6-8.5A^2s. (Neglecting the delay time caused by the hardware circuit) So the actual maximum boundary of $i^2t_{threshold}$ can be redefined as 9A^2s. When plotting the actual interruption characteristic to be compared with the MOSFET's SOA curve as shown in Fig. 17, it can be seen that actual interrupting time of the proposed overcurrent protection scheme is still within the safe zone. On the other hand, the designer could compensate this delay caused by the quantization error by reducing the $i^2t_{threshold}$ when necessary.

5. APPLICATIONS FOR OTHER SPECIFICATIONS

For applying the proposed concept for other systems with different specifications, the design procedure can be listed as follows,

1. Determining the battery type and max. short-circuit current:

Concerning the battery type, Li-Ion battery has the highest capability to supply short-circuit current (up to 20-30C). For other battery types, such as lead-acid battery, the short-circuit current is lower. Basically, there is no major adaptation in the algorithm when using different battery type. The only adaptations are only the current sensing hardware which can be scaled down for less current and the adjustment of the i^2t protection characteristics. Therefore, the designer should consult the datasheet given by the battery manufacturer to determine the maximum short-circuit current by the battery. If it is not available, the maximum short-circuit current can be obtained by experiment.

For larger batteries (larger Ah), the current sensor must be also designed with a larger range corresponding to the larger short circuit current. However, the i^2t short-circuit protection characteristic will not depend on the battery size since it is determined by the SOA of the MOSFETs in the motor converter. But the overload protection should be adjusted to a higher level since the larger battery can supply more overload current. For battery packs with higher voltage rating, the discharging MOSFETs of the BMS must be replaced with a sufficient blocking voltage.

2. Checking the rating of the protection MOSFET in the BMS:

From the battery voltage and the maximum short circuit current, the protection MOSFETs must have sufficient voltage and current rating. In case of very high short-circuit current, more MOSFETs are connected in parallel to gain more current rating.

3. Scaling the current sensor, A/D and computational resource based on overload current:

From the maximum battery current, the current sensor must be scaled appropriately. It is not necessary to measure the peak of the short-circuit current but the maximum measureable current range must be large enough to cover the overload current level.

4. Acquiring the SOA of the used MOSFETs in the converter.

5 Determining the i^2t to cover the SOA of the used MOSFETs but faster than fuse.

6 Adjusting the i^2t algorithm by the number of sampling and the i^2t constant so that the desired protection characteristic is obtained.

6. COMPARISON OF COST AND WEIGHT

This section discusses the comparison in terms of cost and weight of the proposed BMS concept. For the comparison of hardware cost, weight and size, the proposed protection concept requires an additional processing unit and its voltage supply, whereas other components in the developed BMS are identical to the

conventional medium-grade BMS, e.g. current sensor, voltage sensor, charging and discharging MOSFETs.

For the consideration of cost, the processing unit costs roughly 3 USD and its power supply circuit costs roughly 2 USD. Therefore, the cost estimation for the proposed concept will be based on the cost of the conventional BMS plus the cost of the additional hardware of 5 USD. The conventional medium-grade BMS for 36V-Li-Ion pack can be found in the market in the price range of 10-20 USD depending on the quality as shown in Table 3. As a conclusion, the proposed BMS could be more expensive than the conventional BMS in the range of 25-50%.

Table 3: *Comparison of Cost Estimation.*

Cost estimation of medium grade BMS for 36V Li-Ion pack	Hardware cost estimation for the proposed concept for upgrading the BMS
10-20 USD	10-20 USD+5 USD

For the comparison of hardware weight and size, the proposed protection concept requires an additional processing unit and its voltage supply, whereas other components in the developed BMS are identical to the conventional BMS, e.g. current sensor, voltage sensor, charging and discharging MOSFETs. So an additional space on the PCB is needed for the processing unit and its power supply. Therefore, the size of the PCB for the proposed BMS will be roughly 20-30% larger than the conventional one which has an average size of 4cm ×6 cm. But the heat-sink which is the major factor of weight can still be the same size. As a result, the total hardware weights between the developed BMS and the conventional one are quite comparable.

7. CONCLUSION

The overcurrent protection concept was developed and implemented as one software adaptation in a high-grade BMS without additional hardware adaptation. The current-time protection characteristics are designed based on the technical requirements of the Li-Ion battery pack in electric bicycles. Using the proposed concept, the semiconductor devices in the motor converter such as MOSFETs can be fully protected from short-circuit faults on the motor side or inside the motor converter. In addition, the fast interrupting response by the proposed scheme helps reducing the overshoot of the short-circuit current. This minimizes the stress to other components in the short-circuit path, i.e. cables, terminals, connectors etc.

Using the conventional BMS, the converter will be destroyed as well when the motor has short-circuits in windings. Using the proposed concept, the converter will be fully protected. Then, the bicycle owners pay less for the reparation in such case.

8. ACKNOWLEDGEMENT

This publication is one of the results in an industrial-oriented R&D project under cooperation with LA-Ride Co., Ltd. (Thailand).

References

[1] Henry Graber, (2013, Sept), *China's electric bicycle boom: will the fashion last?, Chinadialogue.*, [Online] available: https://www.chinadialogue.net/article/show/single/en/6372-China-s-electric-bicycle-boom-will-the-fashion-last

[2] A. Muetze, and Y. C. Tan, "Performance evaluation of electric bicycles," *Ind. Applicat. Conf. 2005. Fortieth IAS Annual Meeting. Conf. Record 2005*, 2005, pp. 2865-2872.

[3] D. Andrea, *Battery Management Systems for Large Lithium-Ion Battery Packs.*, Massachusetts: Artech House, 2010.

[4] J. Chatzakis, K. Kalaitzakis, N.C. Voulgaris, and S. N. Manias, "Designing a new generalized battery management system", *IEEE Trans. Ind. Electron.*, vol. 50, no. 5, pp. 990-999, Oct. 2003.

[5] J. Garche, and A. Jossen, "Battery management systems (BMS) for increasing battery life time", *The Third Int. Telecommun. Energy Special Conf.*, 2000, pp. 81-88.

[6] M.T. Lawder, B. Suthar, P.W.C. Northrop, S. De, C.M Hoff, O. Leitermann, M.L. Crow, S. Santhanagopalan, and V.R. Subramanian, "Battery energy storage system (BESS) and battery management system (BMS) for grid-scale applications", *Proc. IEEE*, vol. 102, no. 6, pp. 1014-1030, Jun. 2014.

[7] A. Manenti; A. Abba, A. Merati, S.M. Savaresi, and A. Geraci, "A new BMS architecture based on cell redundancy", *IEEE Trans. Ind. Electron.*, vol. 58, no. 9, pp. 4314-4322, Sept. 2011.

[8] FerrazShawmut. *Power Semiconductor Fuse Application Guide.* [Online] available: http://www.ipdgroup.com.au/WMS/Upload/Resources

[9] H. C. Cline, "Fuse protection of DC systems," *Ann. Meeting American Power Conf.*, 1995, pp. 1-6.

[10] T. M. Crnko, "Current-limiting fuse update-new style fuse for protection of semiconductor devices," *IEEE Trans. Ind. Appl.*, vol. IA-15, no. 3, pp. 308-312, May/Jun. 1979.

[11] A. K. Khargekar, and P. P. Kumar, "A novel scheme for protection of power semiconductor," *IEEE Trans. Ind. Electron.*, vol. 41, no. 3, pp. 344-351, Jun. 1994.

[12] C. Meyer, and R. W. De Doncker, "Solid-state circuit breaker based on active thyristor topologies," *IEEE Trans. Power Electron.*, vol. 21, no. 2, pp. 450-458, Mar. 2006.

[13] R. Mehl, and P. Meckler, "Comparison of advantages and disadvantages of electronic and mechanical Protection systems for higher Voltage

DC 400 V", *Proc. 2013* 35^{th} *Int. Telecommun. Energy Conf. Smart Power Efficiency*, 2013, pp. 1-7.

[14] Y. Sato, Y. Tanaka, A. Fukui, M. Yamasaki, and H. Ohashi , "SiC-SIT circuit breakers with controllable interruption voltage for 400-V DC distribution systems", *IEEE Trans. Power Electron.*, vol. 29, no. 5, pp. 2597-2605, May 2014.

[15] A123 System. *Datasheet High Power Lithium Ion APR18650* [Online] available: http://www.a123systems.com

[16] J. Schoiswoh. (June, 2010). *Linear mode operation and safe operating diagram of power MOSFETs* [Online]. available: http://www.infineon.com

[17] NXP, (August 2012). *Understanding power MOSFET datasheet para-meters* [Online]. Available: http://www.nxp.com

[18] *International Rectifier Datasheet*, IRF2807, 2001.

[19] R. H. Kaufmann, "1967 the magic of I^2t", *IEEE Trans. Ind. Appl.*, vol. IA-20, no. 4, pp. 1087,1087, Jul. 1984.

Nisai H. Fuengwarodsakul received his Bachelor of Electrical Engineering in 1998 from King's Mongkut University of Technology North Bangkok and his Master of Science and Doctoral Degree in Electrical Power Engineering in 2001 and 2007 from RWTH-Aachen University, respectively. Since July 2007, he is with The Sirindhorn International Thai-German Graduate School of Engineering, King's Mongkut University of Technology North Bangkok as a lecturer/researcher. His research activities are in the area of electrical drives, battery and electric vehicles. He is member of the IVVBS (Informations Vagabundierende Vektoren Bauern-Seilschaft).

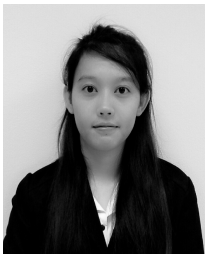

Waraporn Puviwatnangkurn received her Bachelor of Electrical Engineering in 2008 from King Mongkut's University of Technology North Bangkok and her Master Degree of Science in Electrical Power Engineering in 2013 from The Sirindhorn International Thai-German Graduate School of Engineering (TGGS), King Mongkut's University of Technology North Bangkok, respectively. Since November 2013, she has been a researcher in the Electrical Power Engineering Department of TGGS. Her research activities are in the field of electrical energy conversion, battery management system and smart home/building system.

Bundit Tanboonjit received his Bachelor of Electrical Engineering in 2006 from King Mongkut's University of Technology North Bangkok and his Master Degree of Science in Electrical Power Engineering in 2008 from The Sirindhorn International Thai-German Graduate School of Engineering (TGGS), King Mongkut's University of Technology North Bangkok respectively. He worked as a software engineering at Toyota Tsusho Electronics Thailand Company in April 2006. Since December 2006, he has been with The Sirindhorn International Thai-German Graduate School of Engineering, King Mongkut's University of Technology North Bangkok as researcher. He is interested in the research field of electrical drives, battery management system and charger, electric vehicles and embedded system.